Robert L. Amaro[2]
Department of Mechanical Engineering,
University of Alabama,
401 7th Avenue,
Tuscaloosa, AL 35487
e-mail: Robert.amaro67@gmail.com

Ryan M. White
Applied Chemicals and Materials Division,
National Institute of Standards and Technology,
325 Broadway m/s 647,
Boulder, CO 80305
e-mail: Ryan.white@nist.gov

Chris P. Looney
Department of Mechanical Engineering,
Colorado School of Mines,
1812 Illinois Street,
Golden, CO 80401
e-mail: clooney@mymail.mines.edu

Elizabeth S. Drexler
National Institute of Standards and Technology,
Applied Chemicals and Materials Division,
325 Broadway m/s 647,
Boulder, CO 80305
e-mail: elizabeth.drexler@nist.gov

Andrew J. Slifka
Mem. ASME
Applied Chemicals and Materials Division,
National Institute of Standards and Technology,
325 Broadway m/s 647,
Boulder, CO 80305
e-mail: andrew.slifka@nist.gov

Development of a Model for Hydrogen-Assisted Fatigue Crack Growth of Pipeline Steel[1]

Hydrogen has been proposed as a potential partial solution to the need for a clean-energy economy. In order to make this a reality, large-scale hydrogen transportation networks need to be engineered and installed. Steel pipelines are the most likely candidate for the required hydrogen transportation network. One historical barrier to the use of steel pipelines to transport hydrogen was a lack of experimental data and models pertaining to the fatigue response of steels in gaseous hydrogen. Extensive research at NIST has been performed in conjunction with the ASME B31.12 Hydrogen Piping and Pipeline committee to fill this need. After a large number of fatigue crack growth (FCG) tests were performed in gaseous hydrogen, a phenomenological model was created to correlate the applied loading conditions, geometry, and hydrogen pressure to the resultant hydrogen-assisted fatigue crack growth (HA-FCG) response of the steels. As a result of this extensive data set, and a simplification of the above-mentioned phenomenological model, the ASME B31.12 code was modified to enable the use of higher strength steels without penalty, thereby resulting in the potential for considerable installation cost savings. This paper details the modeling effort that led to the code change. [DOI: 10.1115/1.4038824]

Introduction

Hydrogen will likely play a key role in transitioning the world away from the use of fossil fuels as a primary energy source. There are multiple ways in which hydrogen may be used to accomplish this goal. First, hydrogen may be produced with excess power at solar, wind, and other clean power-generation facilities that produce power regardless of demand. In this way, the excess energy generated during times of off-peak demand may be stored as hydrogen. The hydrogen would then be transported throughout the U.S. to be converted to usable energy via electrochemical fuel cells once demand arises. As a second option, hydrogen may be used as a simple energy carrier, i.e., hydrogen production and distribution for the sake of distributed electricity generation rather than simply as an energy storage mechanism. In either scenario, hydrogen must be transported long distances in order for it to achieve its potential usefulness.

Steel pipelines are the most economical means of transporting fuels in the U.S., including hydrogen [1]. Currently, the length of hydrogen-dedicated pipelines in the U.S. comprises only one-half of one percent of the total length of operating U.S. natural gas pipelines [2,3]. Considering the current U.S. natural gas transportation system as a benchmark, one recognizes the need for far more hydrogen-specific pipelines to be operational in the near future in order to meet similar energy needs. According to the ASME B31.12 committee on hydrogen piping and pipelines, a major barrier to the design and installation of steel pipelines for hydrogen transportation has historically been the lack of information on hydrogen-assisted fatigue crack growth (HA-FCG) in pipeline materials. Though noncyclic fracture studies of pipeline steels in gaseous hydrogen have been performed to provide a baseline understanding of the effect of hydrogen upon these loading and failure scenarios [4–8], test results on HA-FCG were lacking because of the expense and difficulty associated with the tests. As such, the ASME committee tasked with creating the hydrogen transportation pipeline design and engineering criteria based the original ASME B31.12-2008 code [9] on the relative response of pipeline steels to monotonic loading in a gaseous hydrogen environment.

An inverse relationship was found between material strength and the adverse effect of hydrogen on ductility, known as hydrogen embrittlement, in tensile tests. Therefore, the use of monotonic data resulted in design thickness penalties, which were assessed to any steel having a specified minimum yield strength (SMYS) greater than 360 MPa (52 ksi). Research at NIST and Sandia National Laboratories, however, has shown that unlike other material properties (e.g., ductility), strength is not correlated to the response of a material to HA-FCG [10]. The recent HA-FCG results produced by the two laboratories indicate that the

---

design penalty placed upon higher strength steels is overly conservative and without justification. Studies have shown that allowing pipeline steels with a SMYS of up to 480 MPa (70 ksi) without penalty could reduce material and installation costs by approximately 25% [11]. As a result, the forthcoming version of the ASME B31.12 code will remove the design penalties on materials with a SMYS between 360 MPa and 480 MPa (52 ksi and 70 ksi). This work details the recent data analysis and modeling studies performed at NIST that were used to inform the ASME B31.12 committee during the code revision process. This work also outlines the HA-FCG modeling background and implementation for both predictive and engineering design purposes.

Hydrogen-Assisted Fatigue Crack Growth Results

The HA-FCG experiments performed at NIST include pipeline base materials, which have a SMYS between 360 MPa and 690 MPa (52 ksi and 100 ksi), as well as on welds and heat-affected zones in pipeline steels with an SMYS between 360 MPa and 480 MPa (52 ksi and 70 ksi). A selection of the data collected at NIST on the base materials from pipeline steels is shown in Fig. 1 [12–14]. The data in Fig. 1, and those in Refs. [12], [13], and [15–17] indicate that the presence of hydrogen can increase the fatigue crack growth rate (FCGR) of pipeline steels as much as an order of magnitude over the FCGR in air, depending upon the applied load and geometry (ΔK). The HA-FCG results also indicate that the effect of hydrogen on the FCG is not dependent upon SMYS, at least between values of 360 MPa (52 ksi) and 690 MPa (100 ksi), as the "X52 New" material at 5.5 MPa data falls right on the response of X70B at 5.5 MPa, for example.

The data presented in Fig. 2 are delineated by the American Petroleum Institute (API) steel designation (e.g., X52), NIST internal naming convention if applicable (e.g., Alloy J, Vintage, New), and hydrogen pressure in MPa. Note that the API naming convention includes the SMYS of the material such that X52 designates an API pipeline steel that has an SMYS of 360 MPa (52 ksi). Fatigue crack growth (FCG) data shown in these figures have da/dN as the dependent variable (y-axis), which is the crack growth per load cycle, and ΔK is the independent variable (X-axis), where ΔK is the stress-intensity-factor range. When delineating the results by material type, there appears to be a correlation between increased hydrogen pressure and increased HA-FCG, shown in Fig. 3(a).

For modeling purposes, analysis of the data in Figs. 1–3 shows that (a) HA-FCG is increased over FCG in air for ΔK values larger than some threshold value, (b) HA-FCG rates are not SMYS dependent, (c) HA-FCG rates appear to increase with hydrogen pressure for a given material, and (d) the HA-FCG data appear to have multiple linear regions of FCG response (shown specifically in Fig. 4). A full description of the HA-FCG test methodology, tests performed, and test results produced at NIST, can be found in Ref. [18].

Fatigue Crack Surface Morphology

Figure 4 details the separation of the HA-FCG response of an API X100 pipeline steel into three regions for discussion purposes. The regions are referred to as regions A, B, and C. The curve for air falls outside the three regions.

In these three regions in Fig. 4, the fracture surfaces produced as a result of the HA-FCG within each region differ markedly. For reference, Fig. 5 provides the FCG surfaces of three representative pipeline materials tested in hydrogen. The ΔK values delineating each region are approximated in the following discussion. The FCG surface in region A ($\Delta K < \sim 8$ MPa m$^{1/2}$) closely matches that produced in air. The response in region B (~ 8 MPa m$^{1/2}$ $< \Delta K < \sim 15$ MPa m$^{1/2}$) produces an FCG surface dominated by crystallographic faceting, indicative of a more brittle FCG response and some hydrogen attack at grain boundaries. Representative crystallographic facets are indicated by arrows in this regime for all three materials shown in Fig. 5. The FCG surface produced in region C ($\Delta K > \sim 15$ MPa m$^{1/2}$), while also exhibiting a small amount of crystallographic faceting, shows a return to much of the character of the FCG surface of air. That is, the existence of quasi-cleavage and "river" marks, as well as the relative amount of crack branching within region C, more closely resembles that of region A. The FCG surface in region C is indicative of a transition to a more ductile fatigue behavior, in contrast to that produced in the middle regime (region B). Specifically, the failure surface morphology in region C indicates that the effect of hydrogen has effectively saturated, in which case the failure surface morphology in region C has components of maximum hydrogen-induced damage (region B) plus an additional ductile-type character similar to that found in region A. The HA-FCG surfaces produced from the different regions for three representative materials are shown in Fig. 5. The FCG surface morphologies found here are similar to those detailed in Refs. [19–21]. Details of quasi-brittle fatigue fracture of a low-carbon steel in hydrogen, where predominantly transgranular cracking was seen, showed that what appeared to be brittle fracture was a combination of extensive slip and localized ductile cracking [22]. An explanation of microstructural details of quasi-cleavage
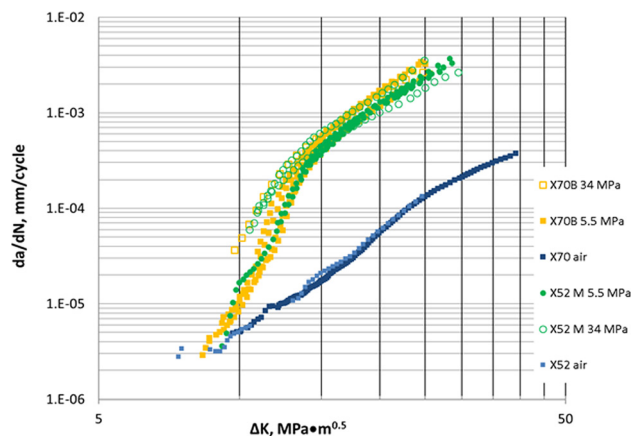
Fig. 1 HA-FCG data collected at NIST on X52 and X70 steels showing the large increase in FCGR for tests in hydrogen at both 5.5 MPa and 34 MPa, compared to tests in air. All data generated at a frequency of 1 Hz and $R = 0.5$.
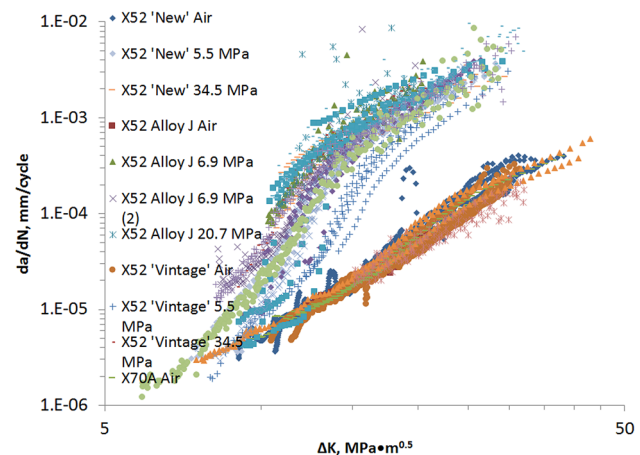

Fig. 2 HA-FCG data collected at NIST on X52, X70, and X100 steels with a SMYS between 358 MPa and 689 MPa at hydrogen pressures between 1.7 MPa and 34.5 MPa. All data generated at a frequency of 1 Hz and $R = 0.5$.
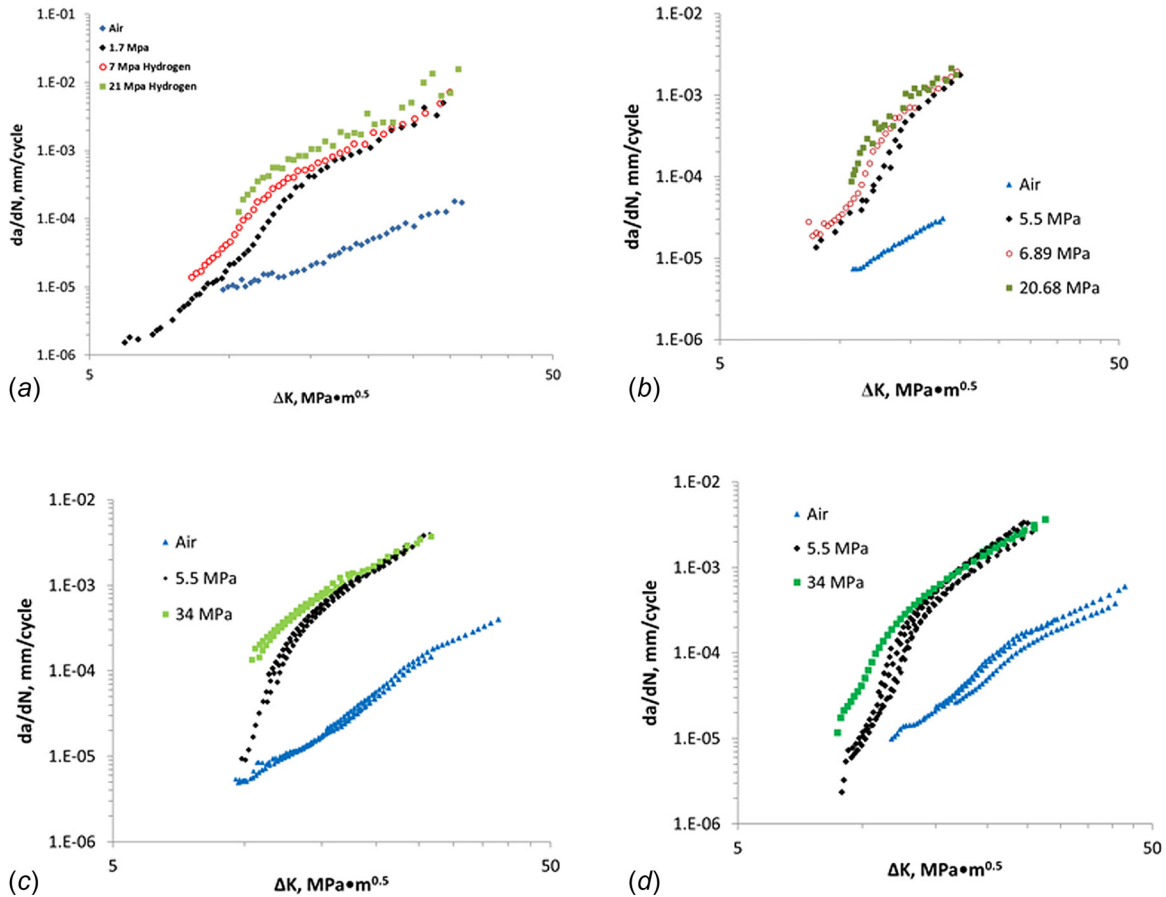
Fig. 3 Representative HA-FCG data of four different API pipeline steels at differing hydrogen pressures, all at 1 Hz: (a) X100, (b) X52 Alloy J, (c) X70A, and (d) X70B. All data generated at a frequency of 1 Hz and $R = 0.5$.

with crystallographic faceting in a low-carbon steel tested in hydrogen gas can be found in the literature [17].

Not only do the images in Fig. 5 indicate a transition in relative amounts of crystallographic faceting between the three regions, the images also indicate a change in the out-of-plane crack branching as a function of crack growth. Crack branching is manifested in Fig. 5 as fissures that traverse into the pictures. As an example, region A exhibits little or no crack branching, region B exhibits considerable branching, while region C exhibits some amount of out-of-plane branching between that of regions A and B for all three materials. This supports the notion of a transition in FCG morphology as the crack traverses the specimen (growing from region A to B to C). It is understood that the HA-FCGR of pipeline steels is sensitive to loading frequency. The test frequency presented here, 1 Hz, was chosen as it provides baseline for understanding of the deformation mechanisms present, while providing a sufficient amount of time for hydrogen diffusion during each loading incursion. A complete discussion of the test frequency as it applies to pipeline operation is provided in Ref. [18].

Dominant Damage Mechanisms

Each of the three regimes discussed above is produced as a result of different dominant damage mechanisms. Each damage mechanism dominates at different times depending upon the rate of crack growth per cycle (da/dN). Given that the FCG regime of region A ($\Delta K < \sim 8$ MPa m$^{1/2}$) produces a fatigue surface that matches that of tests in air, it is presumed that this FCG regime is dominated by a fatigue-only mechanism. Suresh and Ritchie hypothesized that there exists a threshold stress

intensity value, K_{max}^T, below which hydrogen does not affect the FCG response of steels [21]. It is believed that the region A results are due to the stress intensity factor falling below the threshold value, K_{max}^T.

It is understood that the combined HA-FCG response (region A + region B + region C) results from the superposition of a mechanism not affected by hydrogen (region A) and a FCG response affected by hydrogen (region B + region C). This
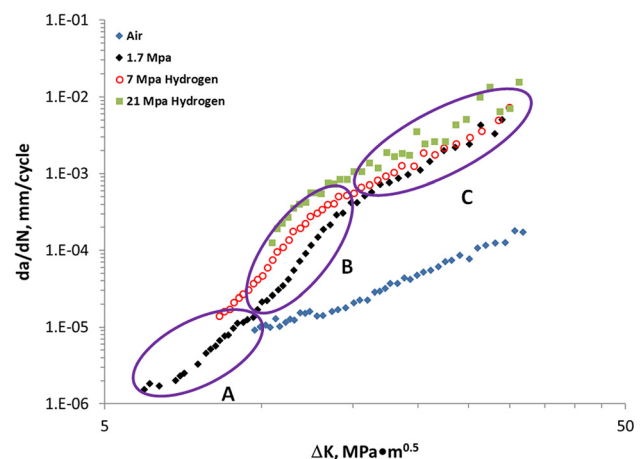

Fig. 4 Typical HA-FCG results of API X100 steel delineated into three regions: A, B, and C. All data generated at a frequency of 1 Hz and $R = 0.5$.

overarching formulation follows the underpinnings of Ref. [23]. The HA-FCG response that is affected by the presence of hydrogen, region B + region C, is comprised of a bi-linear trend when plotting da/dN versus ΔK, which will be discussed further. Similar bi-linear trends, or transitions in FCG response, have been attributed to the following interactions:

- Crack growth beyond the short-crack regime exhibited by most crystalline metals, i.e., crack extension per cycle greater than the material's grain size [24].
- Crack extension per cycle greater than the Widmanstatten packet size for titanium alloys [24].

In both cases, the transition between bi-linear trends in FCGRs results from an interaction between the length of crack extension per cycle and a characteristic length scale of the material microstructure. In the case of HA-FCG, it is believed that the characteristic length scale that determines the transition between region B and region C of HA-FCG, x_{tr}, is a function of the cyclic plastic zone, or fatigue process zone (FPZ) size. The FPZ is the region in front of the crack tip that experiences large-scale plasticity as a result of cyclic loading. This zone is also associated with high levels of hydrostatic stress. Experimental results indicate that the characteristic transition length, as a function of the fatigue process zone size, r, is on the order of

$$x_{tr} \propto 6r \tag{1}$$

where the Irwin estimate of the FPZ size [25] is defined as a function of the material yield strength σ_y by

$$r = \frac{\left(\frac{K_{max}}{\sigma_y}\right)^2}{6\pi} \tag{2}$$

where the variable K_{max} is the maximum stress intensity factor and is related to ΔK by

$$K_{max} = \frac{\Delta K}{1 - R} \tag{3}$$

where R is the load ratio of the test and is defined as $R = K_{min}/K_{max}$. Equation (1), by use of Eq. (2), is plotted as a dashed line along with the HA-FCG results of API X100 steel in Fig. 6.

(a) X52 New, 800 psi (5.5 MPa) hydrogen, 1 Hz

(b) X52 Alloy J, 1000 psi (6.9 MPa) hydrogen, 1 Hz

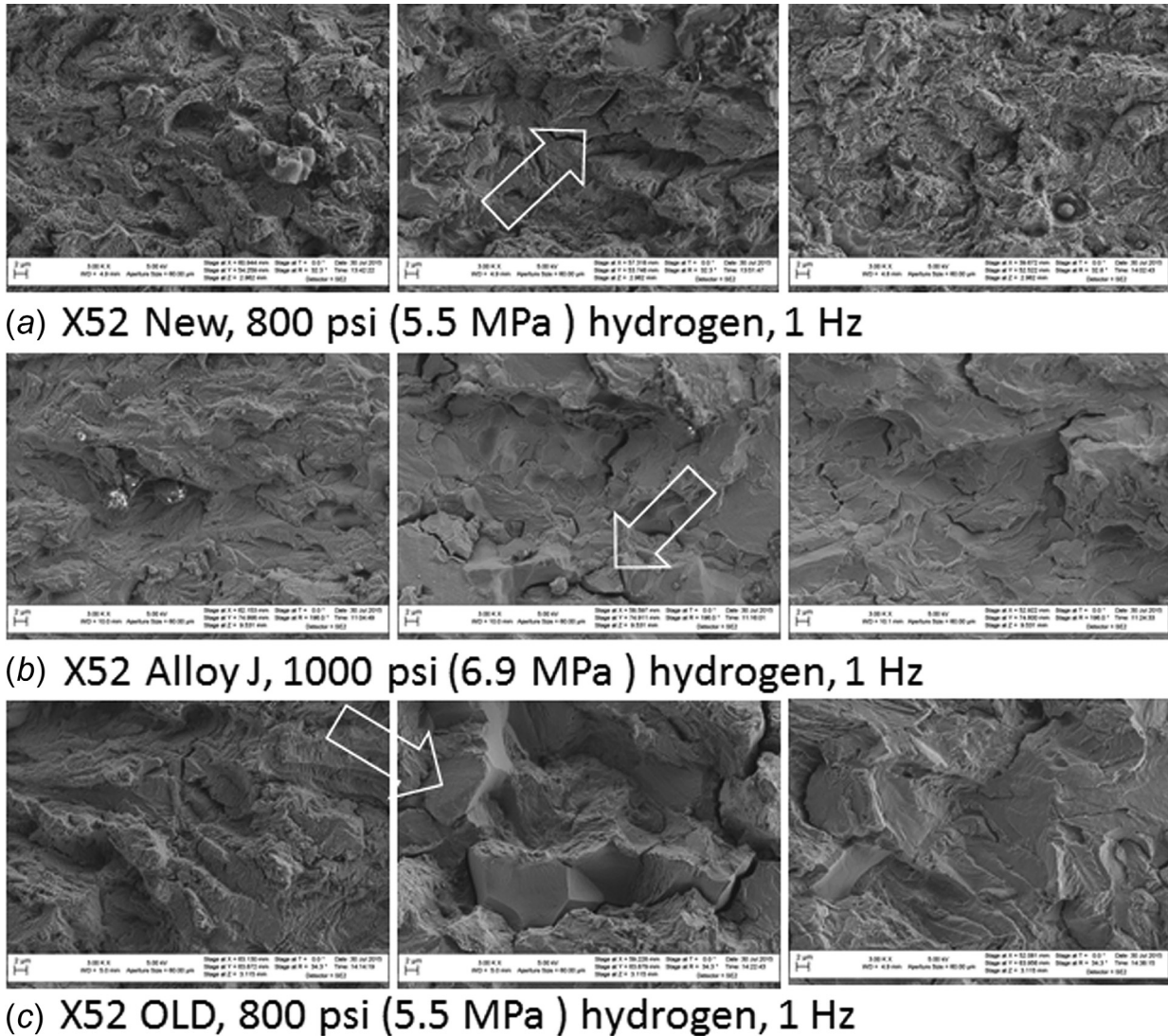(c) X52 OLD, 800 psi (5.5 MPa) hydrogen, 1 Hz

Fig. 5   Fatigue-crack surfaces for three materials tested in gaseous hydrogen (frequency of 1 Hz and $R = 0.5$). The left pictures are of region A, the middle pictures are of region B, and the right pictures are of region C for all materials.
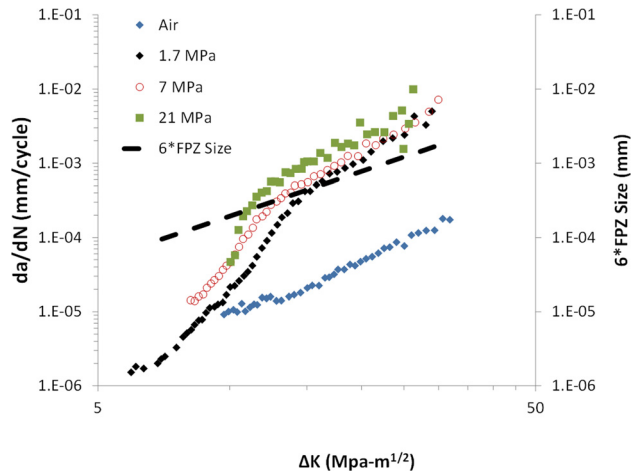
Fig. 6 HA-FCG data for X100 tested in air and three hydrogen pressures superimposed with six times the magnitude of the per-cycle size of the Irwin FPZ as a function of ΔK. All data generated at a frequency of 1 Hz and $R = 0.5$.

Equation (1) correlates well with the transition between the two bi-linear HA-FCG regimes (region B and region C). It is hypothesized here that when the value of da/dN is smaller than x_{tr}, the HA-FCG response is dominated by the stress-assisted hydrogen accumulation within the FPZ. Specifically, while hydrogen accumulation far-field in front of the crack tip is increased due to hydrostatic stresses, the hydrogen concentration within the FPZ is exponentially proportional to the hydrostatic stress. As such, when the da/dN is within the zone of increased hydrogen concentration produced by the $1/r$ dependence of the hydrostatic stress, the FCG falls in region B and is termed the transient HA-FCG regime. Transient is used here given that these materials exhibit this particular HA-FCG response for a finite amount of crack extension per cycle. The presumed interaction between da/dN and the FPZ, which produces the response in the transient regime, is shown graphically in Fig. 7(a). Specifically, when the crack extension, per cycle, falls within the FPZ having size x_{tr}, the resulting FCGR is enhanced. In which case, the presence of the accumulated hydrogen at the crack tip dominates the damage response in

this HA-FCG regime. This results in a more brittle material response than that produced in the region A, ultimately leading to an FCG surface that is dominated by crystallographic faceting. While crack extension per cycle within region A also occurs within the FPZ and its associated region of increased hydrogen concentration, it is hypothesized that the HA-FCGR is not increased over that of air because the critical K-value for environmental-assisted mechanisms to occur (termed K_{max} by Suresh and Ritchie [21]) has not yet been reached.

On the other hand, when the crack extension per cycle, da/dN, extends beyond the FPZ transition length, x_{tr}, with its associated enhanced hydrogen accumulation, the crack extension is affected primarily by the far-field hydrogen accumulation in the material. This leads to the HA-FCG response that is dominated by traditional fatigue mechanisms; albeit at an accelerated rate due to the initial crack extension per cycle occurring within the FPZ. This hypothesis is supported by the evidence that the FCG surface in this regime closely matches that of FCG surfaces tested in air. This HA-FCG regime (region C) is termed the steady-state regime. The relationship between the per-cycle crack extension and the FPZ that correlates to region C is shown in Fig. 7(b). Specifically, in this regime, the per-cycle crack extension grows through and extends beyond the FPZ. While the FCG surface produced by this regime appears to be mixed mode, it exhibits far more transgranular crack growth than intergranular, and, therefore, more closely resembles FCG surfaces of materials tested in air.

Predictive Model

Based upon the above findings, a predictive model was sought to correlate the HA-FCGR of API pipeline steels to the applied load and geometry (together defining ΔK), and hydrogen pressure. The purpose of such a model is to predict the remaining useful lifetime of steel components (e.g., pipes), given an understanding of the boundary conditions and initial conditions placed upon the component. The following outlines the derivation of the predictive model intended for that purpose.

The HA-FCG response of API steels appears to follow a multi-linear trend on the conventional log-log axes used to plot FCGR data. As an example, one could argue that the X100 data collected in hydrogen gas pressurized to 1.72 MPa follows a tri-linear trend, as proposed in Fig. 8.
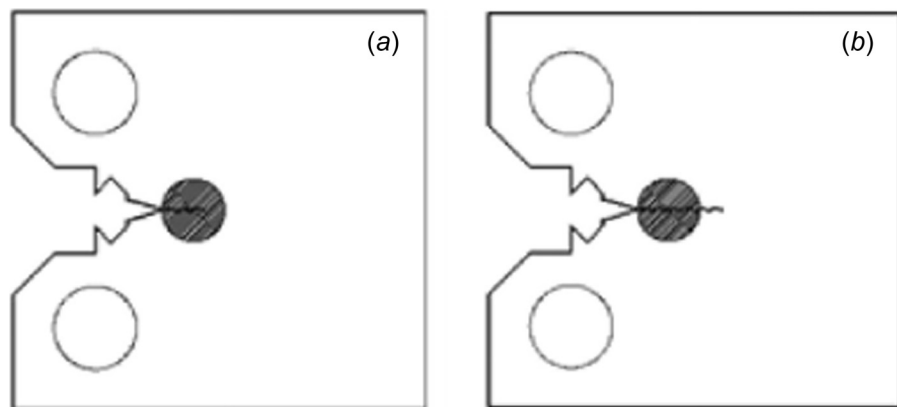
Fig. 7 Exaggerated view of: (a) crack growth per cycle as it occurs within the FPZ of that cycle and the associated region of stress-assisted hydrogen concentration resulting in the transient HA-FCG regime (region B). (b) Crack growth per cycle extending beyond the FPZ of that cycle resulting in the steady-state HA-FCG regime (region C). Fatigue crack shown as emanating from the specimen precrack, and the FPZ shown as a shaded circle for simplicity. Figure 7 depicts a single cycle of crack extension and the associated FPZ occurring at that instance. Each additional cycle will have a new FPZ location associated with the crack tip location at that time.

Figure [8] proposes the existence of one HA-FCG trend for $\Delta K < \sim 8$ MPa m$^{1/2}$, a separate trend for ~ 8 MPa m$^{1/2}$ $< \Delta K < \sim 15$ MPa m$^{1/2}$, and a third trend for $\Delta K > \sim 15$ MPa m$^{1/2}$. In order of increasing ΔK, the three regions are termed the "air," "transient," and "steady-state" regimes for the remainder of this work. These regimes correlate with regions A, B, and C, respectively. Given that the steady-state regime is presumed to be dominated by the same damage mechanisms that occur in air, it is not surprising that the slope of the linear region in the steady-state regime matches that of air.

Based upon the understanding that the FCG response in hydrogen results as a superposition of a fatigue-only component and a hydrogen-assisted component, the following model framework has been proposed:

$$\frac{da}{dN}_{\text{Total}} = \frac{da}{dN}_{\text{air}} + \delta(P_H - P_{H_{th}})\frac{da}{dN}_H \qquad (4)$$

where $(da/dN)_{\text{Total}}$ is the resultant FCG response, $(da/dN)_{\text{air}}$ is the FCG response for the material in air, given by

$$\frac{da}{dN}_{\text{air}} = a\Delta K^B \qquad (5)$$

and $(da/dN)_H$ is the hydrogen-assisted FCG response. The framework outlined in Eq. (4) views the two separate mechanisms as if occurring in parallel; that is, they occur concurrently and without interaction. The Heaviside step function, δ, simply turns the hydrogen FCG response on when the ambient hydrogen pressure, P_H is above a threshold value of $P_{H_{th}} = 0.02$ MPa [26]. Although it is likely that hydrogen affects the FCG response of steels at pressures below 0.02 MPa, this value is used here, as it is the lowest hydrogen pressure for which steel HA-FCG results are known to have been published [27].

As discussed above, the HA-FCG is understood to occur as a result of the interaction between two hydrogen-assisted mechanisms; namely a mechanism dominated by hydrogen accumulation at the crack tip, which results in hydrogen-dominated FCG, and FCG aided by hydrogen, yet dominated by traditional fatigue-in-air damage mechanisms. The HA-FCG response is thought to result from an interaction between a hydrogen-dominated damage mechanism and a damage mechanism dominated by the deformation state at the crack tip. The basis of this modeling technique is derived in the cumulative damage model literature. The cumulative damage reasoning states that if damage mechanisms occur concurrently, the cumulative effect must incorporate damage mechanisms interactions. The two interacting HA-FCG mechanisms are therefore modeled as springs in parallel such that the overall response $(da/dN)_H$ results from whichever mechanism is dominant and thereby providing a damage mechanism as the weak link for crack extension, while also being informed by the less dominant mechanism. The term is defined as

$$\frac{da}{dN}_H = \left[\left(\frac{da}{dN}_{P_H}\right)^{-1} + \left(\frac{da}{dN}_{\Delta K}\right)^{-1}\right]^{-1} \qquad (6)$$

where $(da/dN)_{P_H}$ is the HA-FCG response dominated by the hydrogen accumulation within the FPZ (transient regime), and $(da/dN)_{\Delta K}$ is the HA-FCG response dominated by crack-tip deformation (steady-state regime). The HA-FCG dominated by hydrogen accumulation in the FPZ is given by

$$\frac{da}{dN}_{P_H} = a1\Delta K^{B1}\left(P_H^{m1}\exp\left(\frac{-Q + V\sigma_h}{RT}\right)\right)^{d1} \qquad (7)$$

where Q is the activation energy for hydrogen diffusion ($Q = 27.1$ kJ/mol) [28]; V is the partial molar volume of hydrogen in the metal ($V = 2.0 \times 10^{-6}$ m^3/mol) [29,30]; R is the universal gas constant; T is the absolute temperature; σ_h is the hydrostatic stress at a critical distance in front of the crack tip (Eq. (1)); P_H is the ambient hydrogen pressure; and $a1$, $B1$, $m1$, and $d1$ are fitting parameters. The stress intensity factor is used here to capture the information regarding the crack-tip stress and deformation state for lack of a better surrogate. The stress intensity-driven component of the HA-FCG response was initially described by [19]

$$\frac{da}{dN}_{\Delta K} = a2\Delta K^{B2}\left(P_H^{m2}\exp\left(\frac{-Q + V\sigma_h}{RT}\right)\right)^{d2} \qquad (8)$$

where $a2$, $B2$, $m2$, and $d2$ are fitting parameters and all other parameters are defined above. It was found, however, that the HA-FCG results all converged at larger values of ΔK regardless of the ambient hydrogen pressure, thereby minimizing the effect of the terms within the parenthesis and driving the value of $d2$ toward 0 [31,32]. As such, the following functional form is proposed here for the stress intensity-driven HA-FCG:

$$\frac{da}{dN}_{\Delta K} = a2\Delta K^{B2} \qquad (9)$$

The robust HA-FCG predictive model must be calibrated for each material of interest. A minimum of three FCG tests at three different hydrogen pressures and one FCG test in air are required to calibrate the model. As extrapolation beyond the calibration data is not suggested, all four data sets should be created by use of ΔK values that bound the loading and boundary conditions of interest to be subsequently modeled. Once calibrated, the model can predict HA-FCG as a function of geometry and load (ΔK), as well as hydrogen pressure. If the stress intensity for the geometry of interest is known, e.g., a pipe with an internal thumbnail-shaped crack, one can then use the model to predict the cycles to failure, given particular loading and initial conditions. Furthermore, given a crack of known size and geometry at known stress intensity, one may quantify the effect of an increase or decrease in hydrogen operating pressure upon the lifetime of the component. The full model applied to an X100 pipeline steel is provided in Fig. [9]. Additional implementation examples can be found in Ref. [31]. Model calibrations to several materials are provided in the
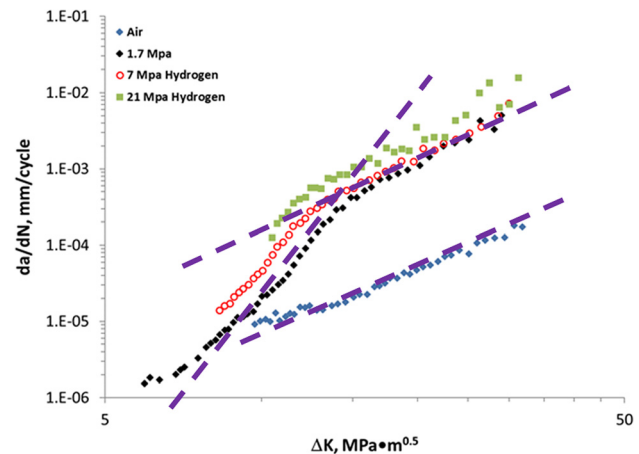

Fig. 8 Three linear trends superimposed upon the HA-FCG of X100 steel. All data generated at a frequency of 1 Hz and $R = 0.5$.
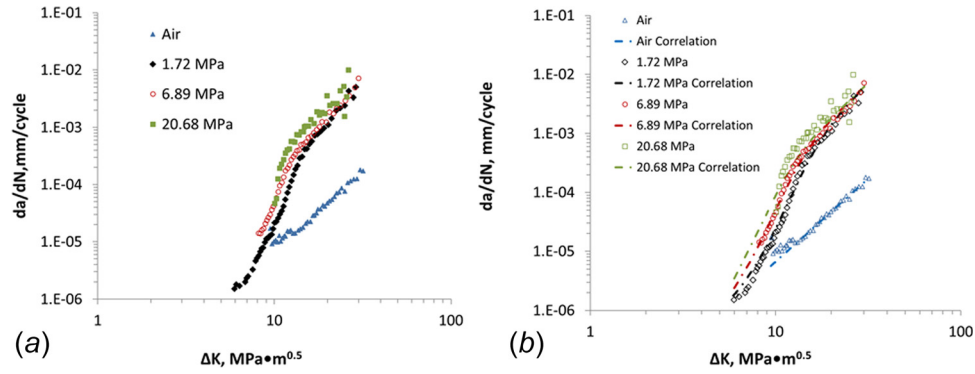
Fig. 9 (*a*) HA-FCG data of API-X100 steel tested in air and three hydrogen pressures, (*b*) model prediction of the data provided in (*a*). Data and predictions for frequency of 1 Hz and *R* = 0.5.

Appendix. When calibrated, the model fits HA-FCGR data to within a factor of 2.

Simplified Model

The full model implementation was presented to the ASME B31.12 committee on several occasions between 2012 and 2015. The committee determined that a simplified engineering version of the model should be developed for potential B31.12 code implementation. The simplified version of the model divides the FCG response into three sections, applies power law relationships to each section, and couples the three sections in the same mathematical framework as the full version of the model [33]. Specifically, the architecture of the simplified model is identical to that of the full version, as shown below:

$$\frac{da}{dN_{\text{total}}} = \frac{da}{dN_{\text{air}}} + \delta(P_H - P_{H_{th}})\frac{da}{dN_H} \tag{10}$$

The first term is again defined by Eq. (5), and the hydrogen-assisted FCG again follows Eq. (6), but the individual terms are simplified as follows:

$$\frac{da}{dN_{P_H}} = a3\Delta K^{B3} \tag{11}$$

and

$$\frac{da}{dN_{\Delta K}} = a4\Delta K^{B4} \tag{12}$$

Note that the simplified model is no longer predictive as a function of hydrogen pressure. As such, model calibrations must be performed for each material of interest, at all hydrogen pressures of interest.

There are two ways in which the simplified model may be calibrated to experimental data. First, power law relationships may be fit to each of the three regions (air, transient, and steady-state), using the relationships in Eqs. (5), (11), and (12). Specifically, the variables *a*, *a*3, *a*4, *B*, *B*3, and *B*4 are all determined as if each region of interest exists independent of the others. When combining the power law relationships in this way, the transitions between each linear region of interest are more gradual, as shown in Fig. 10(*a*). Pseudo code that can be used to create the parameter values *a*, *a*3, *a*4, *B*, *B*3, and *B*4, while minimizing user bias is provided in the Appendix as PseudoCode1.

The second way to calibrate the simplified model is to first fit power law relationships to the three individual regions of interest (as discussed above), followed by a second fitting of the parameters in which the final parameter values for each region are
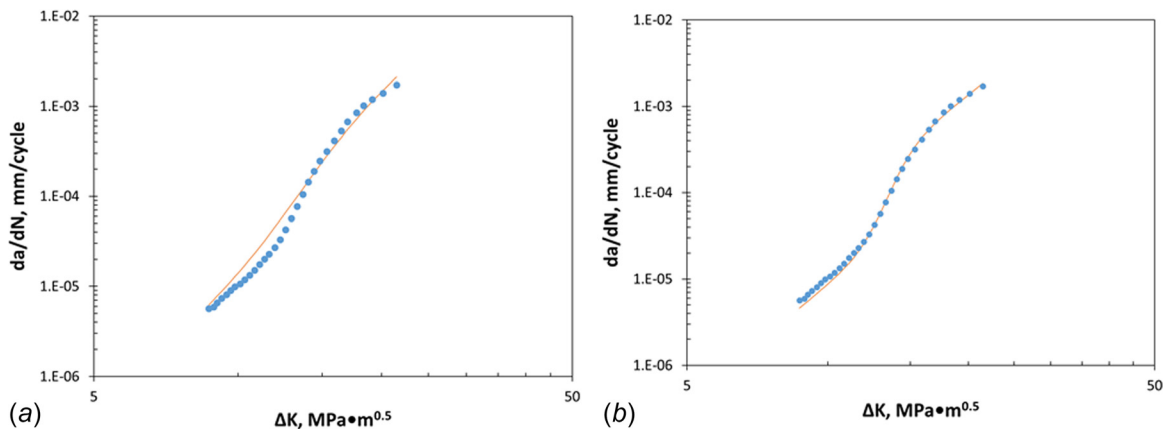

Fig. 10 Simplified fits created by use of API X52 data tested at 1 Hz, *R* = 0.5, in 5.5 MPa gaseous hydrogen. (*a*) Provides the results of a simple fitting of the three regions as if independent, while (*b*) shows the results of enabling a weighting of the three linear fits to more closely match experimental data. Pseudo code for each method is provided in the Appendix.
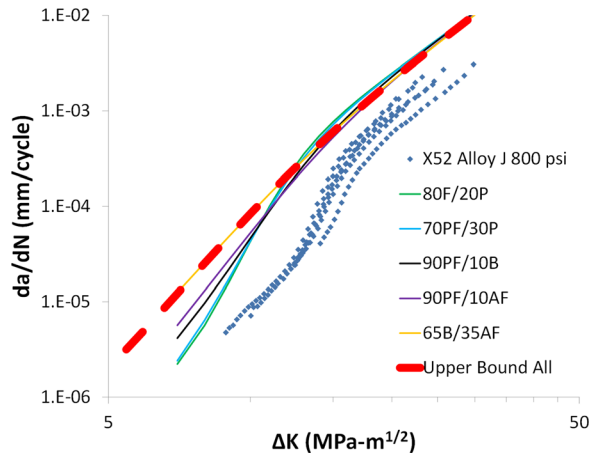
Fig. 11 Implementation of the upper bound of the data to the HA-FCG model as requested by the ASME B31.12 code committee. Data and predictions for a frequency of 1 Hz and $R = 0.5$.
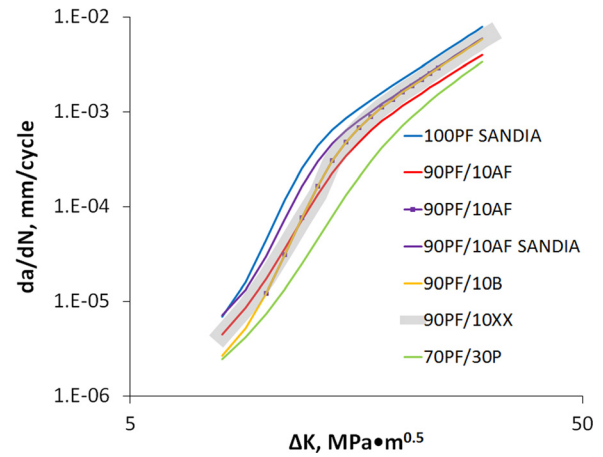

Fig. 12 HA-FCG test results as a function of the material microstructure. PF = polygonal ferrite, AF = acicular ferrite, B = bainite, P = pearlite, XX = all secondary potential constituents. All data generated at a frequency of 1 Hz and $R = 0.5$.

Table 1 Model constants for the upper bound for the ASME B31.12 implementation

		Upper bound for all materials tested			
a	B	$a3$	$B3$	$a4$	$B4$
English (ksi in$^{1/2}$ in/cycle) 2.1746×10^{-10}	3.2106	2.9637×10^{-12}	6.4822	2.7018×10^{-9}	3.6147
Metric (MPa m$^{1/2}$ mm/cycle) 4.0812×10^{-9}	3.2106	4.0862×10^{-11}	6.4822	4.8810×10^{-8}	3.6147

determined by enabling neighboring regions to influence the others. In this way, the calibration more closely fits the transition between regions exhibited by the experimental data. This technique was performed on a representative data set and the results are provided in Fig. 10(*b*). Pseudo code that can be used to create the second-fit parameter values *a*1, *a*3, *a*4, *B*1, *B*3, and *B*4, while minimizing user bias, is provided in the Appendix as Pseudo-Code2 and 3.

While the second calibration technique does a far better job of correlating the data, it is more cumbersome to implement than the first. Simplified model calibrations for all materials tested to date at NIST are provided in the Appendix.

ASME B31.12 Code Implementation

Upon review of both the full and simplified model implementations presented above, the ASME B31.12 committee determined that a single, upper-bound simplification should be employed within the code. That is, given the vast number of microstructural constituents potentially found within pipeline steels and their respective FCGRs (see Fig. 2), the committee determined that use of the worst-case model representation was the safest course of action. Use of this upper bound simplification would then enable the engineer to use materials having SMYS up to 480 MPa (70 ksi) at design pressures up to 20.7 MPa (3000 psi) without penalty. The upper-bound solution utilizes Eqs. (5), (6), and (10)–(12), in conjunction with the parameter values provided in Table 1. The graphical representation of the upper-bound FCG prediction, as well as a representative pipeline steel HA-FCG response, is provided in Fig. 11. Note that the upper bound curve provides an

upper bound for all data tested at NIST, including the data provided in Fig. 2.

Although the upper bound appears to be conservative with respect to the experimental data shown in Fig. 11, it provides an upper bound for all potential HA-FCG data sets in existence for the boundary and loading conditions of interest. As such, one may use the upper-bound model implementation with confidence that the FCG prediction will be conservative for any potential pipeline steel.

Future Work

The full HA-FCG model detailed in Eqs. (4)–(8) can predict the life of a component as a function of hydrogen pressure, provided that (a) there is a closed-form solution for ΔK for the geometry and loading conditions of interest, and (b) the model is calibrated to that particular material. Both provisions are nontrivial. As was detailed in Ref. [31], depending upon which closed-form solution one uses for an internal thumbnail-shaped crack (as an example), the resulting life estimate may be upward of $2\times$ different than if another estimate was chosen. Additionally, full model calibrations require a minimum of one test in air and one test at three different hydrogen pressures for each pipeline steel of interest. As can be seen in Fig. 2 and was discussed previously, the HA-FCG response of pipeline steels is not correlated with their API designation. That is, the HA-FCG response is not correlated to the SMYS of the material. The HA-FCG response does appear to correlate with the microstructure of the material, however. Specifically, the HA-FCGR for a material increases with increasing percent polygonal ferrite, as shown in Fig. 12.

To address the two provisions discussed above, NIST is supporting a concerted effort to create and calibrate microstructure-specific models, implemented into a finite element (FE) platform. Once completed, the FE analysis will enable the user to calculate the HA-FCGR for any geometry and loading condition, not just those for which a closed-form K-solution exists. Furthermore, the microstructure-based model will enable the engineer to calculate HA-FCGR for any material, with any microstructure, given that the microstructure of the pipeline material is known. Finally, the implemented FE model would enable material design for improved HA-FCG response.

Summary. This paper, in conjunction with Ref. [18], provides a detailed accounting of the work performed at NIST to support a modification of the ASME B31.12 code to enable the use of higher strength pipeline steels for hydrogen transportation. Specific conclusions from this work are as follows:

- A phenomenological model has been created to predict HA-FCG of pipeline steels. In the simplified engineering form, the model is capable of predicting HA-FCG for each material that it has been calibrated to (see Table 2).

- A single, upper bound solution set of the phenomenological model has been chosen to be implemented within the ASME B31.12 code. While still somewhat conservative, if chosen to be utilized by the design engineer, this model will enable the use of API steels having SMYS up to 70 ksi without penalty.
- The phenomenological model may also be used, in conjunction with the data in Table 2, to enable pipeline design engineers to more accurately predict pipeline-specific HA-FCG for engineering purposes.

Funding Data

Appendix

Simplified model calibrations performed to date are provided in Table 2. Table 3 provides the chemical compositions, tensile properties, and microstructural constituents of all materials in which HA-FCG tests have been performed at NIST.

Table 2 Simplified model calibrations of pipe base materials performed to date

Material	Section	Frequency (Hz)	R-value	Hydrogen pressure (MPa)	Paris prefactor (a_i)	Paris exponent (B_i)
X52 Alloy J	All	1	0.5	0	2.43×10^{-9}	3.3085
	Transient	1	0.5	6.89	1.80×10^{-12}	8.195
	Steady-state	1	0.5	6.86	1.65×10^{-7}	3.224
	Transient	1	0.5	20.68	9.32×10^{-17}	11.696
	Steady-state	1	0.5	20.68	4.88×10^{-8}	3.6147
*	Transient	1	0.5	5.5	6.77×10^{-17}	11.513
*	Steady-state	1	0.5	5.5	1.24×10^{-8}	3.9786
*	Transient	1	0.5	21	1.25×10^{-13}	8.7596
*	Steady-state	1	0.5	21	2.63×10^{-8}	3.757
*	All	1	0.5	0	1.66×10^{-9}	3.6111
X100	All	1	0.5	0	9.84×10^{-9}	2.8285
	Transient	1	0.5	1.72	3.92×10^{-15}	9.5469
	Steady-state	1	0.5	1.72	3.09×10^{-8}	3.5035
	Transient	1	0.5	6.89	6.70×10^{-13}	7.8635
	Steady-state	1	0.5	6.89	1.10×10^{-7}	3.1639
	Transient	1	0.5	20.68	4.09×10^{-11}	6.4822
	Steady-state	1	0.5	20.68	2.40×10^{-7}	3.05
	Transient	0.1	0.5	6.89	9.41×10^{-13}	7.9222
	Steady-state	0.1	0.5	6.89	1.46×10^{-7}	3.2187
X52 New	All	1	0.5	0	1.61×10^{-9}	3.5021
	Transient	1	0.5	5.51	1.59×10^{-12}	7.1574
	Steady-state	1	0.5	5.51	6.80×10^{-8}	3.2774
	Transient	1	0.5	34.47	2.93×10^{-12}	7.3247
	Steady-state	1	0.5	34.47	5.78×10^{-7}	2.5876
X52 Vintage	ALL	1	0.5	0	1.82×10^{-9}	3.3934
	Transient	1	0.5	5.51	2.52×10^{-14}	8.2592
	Steady-state	1	0.5	5.51	4.20×10^{-8}	3.3123
	Transient	1	0.5	34.47	1.13×10^{-15}	10.63
	Steady-state	1	0.5	34.47	1.89×10^{-7}	3.0779
X70B	ALL	1	0.5	0	4.08×10^{-9}	3.2106
	Transient	1	0.5	5.51	1.31×10^{-15}	9.9163
	Steady-state	1	0.5	5.51	2.53×10^{-8}	3.6545
	Transient	1	0.5	34.47	7.58×10^{-14}	8.812
	Steady-state	1	0.5	34.47	2.31×10^{-7}	2.9292
X70A	ALL	1	0.5	0	1.73×10^{-9}	3.4426
	Transient	1	0.5	5.51	4.82×10^{-14}	8.5428
	Steady-state	1	0.5	5.51	3.42×10^{-8}	3.575
	Transient	1	0.5	34.47	—	—
	Steady-state	1	0.5	34.47	4.54×10^{-7}	2.762

Table 3 Chemical compositions, tensile properties, and microstructural constituents of alloys tested at NIST. The *R*-value and B_i are unit less. The units of a_i are $\mathrm{m/cycle(MPa\sqrt{m})}^{Bi}$.

	Al	C	Co	Cr	Cu
X52 Alloy J	0.034	0.06	—	0.03	0.03
X52 Vintage	0.002	0.238	0.004	0.014	0.085
X52 New	0.017	0.071	0.002	0.033	0.016
X70A	0.015	0.048	0.002	0.24	0.22
X70B	0.012	0.053	0.002	0.23	0.25
X100	0.012	0.064	0.003	0.023	0.28
	Fe	Mn	Mo	N	Nb
X52 Alloy J	—	0.87	0.00	—	0.03
X52 Vintage	98.48	0.96	0.004	0.003	0.001
X52 New	98.37	1.06	0.003	0.004	0.026
X70A	97.51	1.43	0.005	0.005	0.054
X70B	97.41	1.53	0.003	0.005	0.054
X100	96.9	1.87	0.23	0.003	0.017
	Ni	P	Si	Ti	V
X52 Alloy J	0.02	0.011	0.12	0.000	0.002
X52 Vintage	0.05	0.011	0.064	0.002	0.002
X52 New	0.016	0.012	0.24	0.038	0.004
X70A	0.14	0.009	0.17	0.027	0.004
X70B	0.14	0.01	0.16	0.024	0.004
X100	0.47	0.009	0.099	0.017	0.002

Material	σ_y MPa (ksi)	σ_{UTS} MPa (ksi)	Pearlite (%)	Polygonal ferrite (%)
X52 Alloy J	442 (64.1)	576 (83.5)	~20	~80
X52 Vintage	325 (47)	526 (76.3)	~30	~70
X52 New	487 (70.6)	588 (85.3)		~90
X70A	553 (80.2)	640 (92.8)		~90
X70B	509 (73.8)	609 (88.3)		~90
X100	689 (99.9)	811 (117.6)		

Material	Acicular ferrite (%)	Bainite (%)	Grain size (um)
X52 Alloy J			~15
X52 Vintage			~10
X52 New	~10		~1
X70A	~10		~1
X70B		~10	~1
X100	~35	~65	

PseudoCode1

Clear all previous data and variables
Prompt user for file
Prompt user for data range within file
Store the Delta K and da/dN data points as variables **x** and **y** respectively
Plot **x** versus **y** data on a logarithmic scale in both axis so that the user can view the data set
Prompt the user to select a point in which they think is part of region 1 the _____ based region
Store this point as variable **PickedPoint**
Create variables **up** and **low** and set both equal to zero
    These will be used to turn on and off specific parts of the tolerance check loop
Create variable **resetBounds** and set equal to 1
    This will be used to turn on and off the loop which determines the initial line fit for a region
Create variable **nextRegion** and set equal to 1
    This variable keeps the program in a large loop until all three regions have been found
Create variable **count** and set equal to zero
    This variable keeps track of how many times the main loop has been executed (how many regions have been found)
Create variable **tolerance** and set equal to desired initial tolerance.
    This will be turned into a percentage later
Create main loop that will run while **nextRegion** is equal to 1
Add one to **count**
Create variable **accepted** and set equal to zero
    This variable will keep the program in the next loop until the user has accepted the fit for the region being worked with
Create variable **stop** and set equal to zero
    This variable will keep the program in the tolerance loop until a point on the fitted line exceeds the set tolerance
Create accepted loop that will run while **accepted** equals zero
Create conditional statement so that program will only advance here if **resetBounds** equals 1
    Create variable **lower** and set equal to **PickedPoint**-1
    Create conditional statement so that if **lower** is less than 1 then **lower** equals 1
        This will keep the tolerance checks from indexing beyond the dataset

Create variable **upper** and set equal to **PickedPoint** + 1

Create conditional statement so that if **upper** is greater than the number of x data points then **upper** equals the highest index of **x**

   This will keep the tolerance checks from indexing beyond the dataset

Create sub set of data **xx** which contains all **x** points from the **lower** index to the **upper** index

Create sub set of data **yy** which contains all **y** points from **lower** index to **upper** index

Find a power fit line ($y = \alpha x^{\beta}$) of (**xx,yy**) and store alpha and beta as variables **a** and **b**

Create variable **yfitstart** and set equal to the y values of the power fit line for x values 1 through the number of **x** points from raw data

End the **resetBounds** section by setting **resetBounds** equal to zero

Create variable **yfit** and set equal to **yfitstart**

Create variable **toleranceAbove** and set equal to 1+(**tolerance**/100)

Create variable **toleranceBellow** and set equal to 1-(**tolerance**/100)

Create a loop that will run as long as stop equals zero

Create conditional statement so that if the **upper** index of **yfit** is greater than **toleranceAbove** times the **upper** index of **y** or less than **toleranceBelow** times the upper index of **y** then setup equal to 1

Create conditional statement so that if the **lower** index of **yfit** is greater than **toleranceAbove** times the **lower** index of **y** or less than **toleranceBelow** times the **lower** index of **y** then set **low** equal to 1

Create conditional statement so if **up** and **low** both equal 1 then **stop** equals 1 which will exit the tolerance checking loop

Create conditional statement so that if **up** equals zero **upper** equals **upper** plus one

Create conditional statement so that if **upper** is greater than the number of x data points then **upper** equals the highest index of **x**

Create conditional statement so that if **low** equals zero **lower** equals **lower** plus one

   Create conditional statement so that if **lower** is less than 1 then **lower** equals 1

Change sub set **xx** to contain all **x** points from the new **lower** index to the new **upper** index

Change sub set **yy** to contain all **y** points from the new **lower** index to the new **upper** index

Find a power fit line ($y = \alpha x^{\beta}$) of (**xx,yy**) and store alpha and beta as variable **a** and **b**

Change variable **yfit** to equal to the y values of the power fit line for x values 1 through the number of **x** points from raw data

On a logarithmic plot in both axis plot (**x,y**) and (**x,yfit**)

   (**x,y**) should be plotted as individual data points. (**x,yfit**) should be plotted as a line

Prompt user for feed back

   Ask user if they accept the fit

   Ask user if they would like to change the picked point

   Ask user if they would like to adjust the tolerance

Create conditional statement so that if the user picked a new point then store the new point as variable **PickedPoint** and set **resetBounds** equal to 1

Create conditional statement so that if the user accepts the fit **stop** equals 1

   Otherwise set **accepted**, **stop**, **up**, and **low** all equal to zero. Set **yfit** equal to **yfitstart**

     Set variable **lower** equal to **PickedPoint**-1

     Create conditional statement so that if **lower** is less than 1 then **lower** equals 1

     Set variable **upper** equal to **PickedPoint** + 1

Create conditional statement so that if **upper** is greater than the number of x data points then **upper** equals the highest index of **x**

Create conditional statement if **count** equals 1

   Create variable **R1upper** and set equal to **upper**

   Create variable **R1lower** and set equal to **lower**

   Create variable **R1yfit** and set equal to **yfit**

   Create variable **a1** and set equal to **a**

   Create variable **b1** and set equal to **b**

   Plot raw (**x,y**) data on a logarithmic scale in both axis so that the user can view the data set

   Prompt the user to select a point in which they think is part of region 2 the _____ based region

   Store this point as variable **PickedPoint**

   Set variable **resetBounds** equal to 1

Create conditional statement if **count** equals 1

   Create variable **R2upper** and set equal to **upper**

   Create variable **R2lower** and set equal to **lower**

   Create variable **R2yfit** and set equal to **yfit**

   Create variable **a2** and set equal to **a**

   Create variable **b2** and set equal to **b**

   Plot raw (**x,y**) data on a logarithmic scale in both axis so that the user can view the data set

   Prompt the user to select a point in which they think is part of region 3 the _____ based region

   Store this point as variable **PickedPoint**

   Set variable **resetBounds** equal to 1

Create conditional statement if **count** equals 3

   Create variable **R3upper** and set equal to **upper**

   Create variable **R3lower** and set equal to **lower**

   Create variable **R3yfit** and set equal to **yfit**

   Create variable **a3** and set equal to **a**

   Create variable **b3** and set equal to **b**

   Set variable **nextRegion** equal to zero

Create variables **R12x** and **R12y** and store the x and y values of the intercept between regions 1&2

Create variables **R23x** and **R23y** and store the x and y values of the intercept between regions 2&3

Preform any required operations required to trim regions to intercepts and combine the three trimmed regions into one x and one y array called **xMeasured** and **yMeasured** respectively.

Create array **ycalculated** and store all y values for all three regions based on the equation_____

Plot on a logarithmic plot in both axis **(x,y)**, **(x,ycalculated)**, **(xMeasured,yMeasured)**

(x,y) should be plotted as individual points. (x,ycalculated) and (xMeasured,yMeasured) should be plotted as solid lines in separate colors

PseudoCode2 and 3- to be used together

PseudoCode2

Clear all previous data, variables, etc.

Call code provided in pseudo code 1 and carry over variables **a1, a2, a3, b1, b2, b3, data, x, ycalculated, xMeasuered,** and **yMeasured.**

Prompt user to answer yes or no to the question "Do you have Paris values for the material ran in air?"

Create variable **air** and set equal to 1 if user entered yes or 0 if user entered no

Create conditional statement for value of **air**

If **air** equals 1

    Prompt user for "Paris prefactor for air" and overwrite **a1** from pseudo code 1

    Prompt user for "Paris exponent for air" and overwrite **b1** from pseudo code 1

Create a 3x2 matrix **data1** and populate with $\begin{bmatrix} a1 & b1 \\ a2 & b2 \\ a3 & b3 \end{bmatrix}$

If **air** equals 0

Create a 3x2 matrix **data1** and populate with $\begin{bmatrix} a1 & b1 \\ a2 & b2 \\ a3 & b3 \end{bmatrix}$

End conditional statement

Create variable **data2** and set equal to **data**

Create cell **data3** and populate with {**data1,data2**}

Create variable **opt_parameteres** and set equal to the output from the function described in pseudo code 3 using **data3** as an input

Plot on a logarithmic plot in both axis **(xMeasured,yMeasured)** and **(x,ycalculated)**

Create variable **airf** and set equal to **opt_parameters**(1,1)*10^(-10) * **data2**(:,1)^**opt_parameters**(1,2)

    Where (1,1) is (row number, column number) and: means all

Create variable **transf** and set equal to **opt_parameters**(2,1) *10^-19 ***data2**(:,1)^**opt_parameters**(2,2)

Create variable **ssf** and set equal to **opt_parameters**(3,1)*10^-10***data2**(:,1).^**opt_parameters**(3,2)

Create variable **fitlifef** and set equal to **airf**+(((**transf**).^(-1)+(**ssf**).^(-1)).^(-1)

Plot on a logarithmic plot in both axis (**data2**(:,1), **fitlifef**) and (**x,y**)

Create variable **piecewise_values** and set equal to **data1**

Create 3x2 matrix **single_function_values** and populate with

$$\begin{bmatrix} \mathbf{opt\_parameters}(1,1){*}10^{\wedge}-10 & \mathbf{opt\_parameters}(1,2) \\ \mathbf{opt\_parameters}(2,1){*}10^{\wedge}-19 & \mathbf{opt\_parameters}(2,2) \\ \mathbf{opt\_parameters}(3,1){*}10^{\wedge}-10 & \mathbf{opt\_parameters}(3,2) \end{bmatrix}$$

PseudoCode3

Create function that takes **data3** as an input and outputs **opt_parameters**

Create variable **data1** and set equal to cell one of **data3**

Create variable **data2** and set equal to cell two of **data3**

Create variable **expnt_air** and set equal to the exponent on **data1(1,1)**

    Where (1,1) is (row number, column number). This format will be used going forward

Create variable **expnt_trans** and set equal to the exponent on **data1(2,2)**

Create variable **expnt_ss** and set equal to the exponent on **data1(3,2)**

Create 3x2 matrix **ab** and populate with $\begin{bmatrix} \mathbf{data}1(1,1){*}10^{\wedge}\mathbf{expnt\_air} & \mathbf{data}(1,2) \\ \mathbf{data}1(2,1){*}10^{\wedge}\mathbf{expnt\_air} & \mathbf{data}(2,2) \\ \mathbf{data}1(3,1){*}10^{\wedge}\mathbf{expnt\_air} & \mathbf{data}(3,2) \end{bmatrix}$

Create 3x2 matrix **lb** and populate with $\begin{bmatrix} \mathbf{ab}(1,1){*}.999 & \mathbf{ab}(1,2){*}.75 \\ \mathbf{ab}(2,1){*}10^{\wedge}-12 & \mathbf{ab}(2,2){*}.9 \\ \mathbf{ab}(3,1){*}.1 & \mathbf{ab}(3,2){*}.75 \end{bmatrix}$

Create 3x2 matrix **ub** and populate with $\begin{bmatrix} \mathbf{ab}(1,1){*}10 & \mathbf{ab}(1,2){*}3 \\ \mathbf{ab}(2,1){*}1.1 & \mathbf{ab}(2,2){*}5 \\ \mathbf{ab}(3,1){*}10 & \mathbf{ab}(3,2){*}1.25 \end{bmatrix}$

Create function that will minimize a residual function **error1** based on **ab**, **lb**, **ub**, with a tolerance 1e-8 and stores the resulting optimized values of **ab** as **opt_parameters**

    Note: an example of such a function is fmincon in MATLAB

Create the residual function **error(params,data2)**

    Where **params** is a variable filled with variable set to be optimized, **ab**. **Params** should be fed back into minimization function until the tolerance is reached.

Create variable **a1** and set equal to **params**(1,1)*10ˆ-10;

Create variable **b1** and set equal to **params**(1,2);

Create variable **a2** and set equal to **params**(2,1)*10ˆ-19;

Create variable **b2** and set equal to **params**(2,2);

Create variable **a3** and set equal to **params**(3,1)*10ˆ-10;

Create variable **b3** and set equal to **params**(3,2);

Create a loop to go from 1 to the number of rows in **data2**

Create variable **air**(index#) and set equal to **a1*****data2**(index #,1)ˆ**b1**

Where index # is the number of times through the loop and **air** will become an array of size 1 x number of rows in **data2**. This format will be used going forward

Create variable **trans**(index #) and set equal to **a2*****data2**(index #,1)ˆ**b2**

Create variable **ss**(index #) and set equal to **a3*****data2**(index #,1)ˆ**b3**;

Create variable **fitlife**(index #) and set equal to **air**(index #)+((**trans**(index #))ˆ(-1)+(**ss**(index #))ˆ(-1))ˆ(-1)

Create variable **residual** (index #) and set equal to **fitlife**(index #)-**data2**(index #,2)

End the loop

References

[1] Furchtgott-Roth, D., 2013, "American Energy Independence, Safety Means More Pipelines," Washington Examiner, Washington, DC, accessed July 10, 2013, http://www.washingtonexaminer.com/american-energy-independence-safety-means-more-pipelines/article/2532854

[2] U.S. DOE, 2008, "The Impact of Increased Use of Hydrogen on Petroleum Consumption and Carbon Dioxide Emissions," U.S. Energy Information Administration, U.S. Department of Energy, Washington, DC, Report No. SR/OIAF-CNEAF/2008-04.

[3] U.S. DOE, 2010, "About U.S. Natural Gas Pipelines-Transporting Natural Gas," U.S. Energy Information Administration, U.S. Department of Energy, Washington, DC, accessed Jan. 3, 2018, http://www.eia.doe.gov/pub/oil_gas/natural_gas/analysis_publications/ngpipeline/index.html

[4] Cialone, H. J., and Holbrook, J. H., 1988, "Sensitivity of Steels to Degradation in Gaseous Hydrogen," Hydrogen Embrittlement: Prevention and Control, ASTM, West Conshohocken, PA, Standard No. ASTM STP 962.

[5] Duncan, A., 2007, "Tensile Testing of Carbon Steel in High Pressure Hydrogen," ASME Paper No. PVP2007-26736.

[6] Nibur, K., Somerday, B. P., Balch, D. K., and San Marchi, C., 2008, "Sustained Load Cracking of Steels for Hydrogen Storage and Delivery," International Hydrogen Conference, Moran, WY, Sept. 7–10, pp. 341–348.

[7] Moro, I., Briottet, L., Lemione, P., Andrieu, E., Blanc, C., Odemer, G., Chene, J., and Jambon, F., 2008, "Damage Under High Pressure Hydrogen Environment of a High Strength Pipeline Steel X80," International Hydrogen Conference, Moran, WY, Sept. 7–10, pp. 357–364.

[8] Xu, K., and Rana, M., 2008, "Tensile and Fracture Properties of Carbon and Low Alloy Steels in High Pressure Hydrogen," International Hydrogen Conference, Moran, WY, Sept. 7–10, pp. 349–356.

[9] ASME, 2012, Hydrogen Piping and Pipelines, American Society of Mechanical Engineers, New York, p. 258.

[10] Slifka, A. J., Drexler, E. S., Stalheim, D. G., Amaro, R. L., Lauria, D. S., Stevenson, A. E., and Hayden, L. E., 2013, "The Effect of Microstructure on the Hydrogen-Assisted Fatigue of Pipeline Steels," ASME Paper No. PVP2013-97217.

[11] Fekete, J. R., Sowards, J. W., and Amaro, R. L., 2015, "Economic Impact of Applying High Strength Steels in Hydrogen Gas Pipelines," Int. J. Hydrogen Energy, 40(33), pp. 10547–10558.

[12] Slifka, A. J., Drexler, E. S., Nanninga, N. E., Levy, Y. S., McColskey, J. D., Amaro, R. L., and Stevenson, A. E., 2014, "Fatigue Crack Growth of Two Pipeline Steels in a Pressurized Hydrogen Environment," Corros. Sci., 78, pp. 313–321.

[13] Drexler, E. S., Slifka, A. J., Amaro, R. L., and Lauria, D. S., 2014, "FCGR of Pipeline Steels in Pressurized Hydrogen Gas: A Comparison of Cyclic Loading Rates," SteelyHydrogen, 2nd International Conference on Metals and Hydrogen, Ghent, Belgium, May 5–7, pp. 403–416.

[14] Slifka, A., Drexler, E. S., Amaro, R. L., Lauria, D. S., Hayden, L. E., Stalheim, D. G., and Chen, Y., 2014, "Summary of an ASME/DOT Project on Measurements of Fatigue Crack Growth Rate of Pipeline Steels," ASME Paper No. PVP2014-28938.

[15] Drexler, E. S., Slifka, A. J., Amaro, R. L., Barbosa, N., Lauria, D. S., Hayden, L. E., and Stalheim, D. G., 2013, "Fatigue Crack Growth Rates of API X70 Pipeline Steel in a Pressurized Hydrogen Gas Environment," Fract. Fatigue Eng. Mater. Struct., 37(5), pp. 517–525.

[16] Slifka, A. J., Drexler, E. S., Rustagi, N., Lauria, D. S., McColskey, D. S., Amaro, R. L., Stalheim, D. G., and Hayden, L., 2012, "Fatigue Crack Growth of Two X52 Pipeline Steels in a Pressurized Hydrogen Environment," International Hydrogen Conference, Moran, WY, Sept. 9–12, pp. 299–307.

[17] Lee, D., Nishikawa, H., Oda, Y., and Noguchi, H., 2013, "Small Fatigue Crack Growth Characteristics and Fracture Surface Morphology of Low Carbon Steel in Hydrogen Gas," Int. J. Fract., 179(1–2), pp. 147–156.

[18] Slifka, A. J., Drexler, E. S., Amaro, R. L., Hayden, L. E., Stalheim, D. G., Lauria, D. S., and Hrabe, N. W., 2018, "Fatigue Measurement of Pipeline Steels for the Application of Transporting Gaseous Hydrogen," ASME J. Pressure Vessel Technol., 140(1), p. 011407.

[19] Amaro, R. L., Findley, K. O., Rustagi, N., Drexler, E. S., and Slifka, A. J., 2014, "Fatigue Crack Growth of X100 Pipeline Steels in Gaseous Hydrogen," Int. J. Fatigue, 59, pp. 262–271.

[20] San Marchi, C., Stalheim, D. G., Somerday, B. P., Boggess, T., Nibur, K. A., and Jansto, S., 2010, "Fracture and Fatigue of Commercial Grade API Pipeline Steels in Gaseous Hydrogen," ASME Paper No. PVP2010-25825.

[21] Suresh, S., and Ritchie, R. O., 1982, "Mechanistic Dissimilarities Between Environmentally Influenced Fatigue-Crack Propagation at Near-Threshold and Higher Growth Rates in Lower Strength Steels," Met. Sci., 16(11), pp. 529–538.

[22] Takahashi, Y., Nishikawa, H., Oda, Y., and Noguchi, H., 2010, "Microscopic Characterization of Hydrogen-Induced Quasi-Brittle Fatigue Fracture in Low-Strength Carbon Steel," Mater. Lett., 64(22), pp. 2416–2419.

[23] Wei, R. P., and Gao, M., 1983, "Reconsideration of the Superposition Model for Environmentally Assisted Fatigue Crack Growth," Scr. Metall., 17(7), pp. 959–962.

[24] Hertzberg, R. W., 1996, Deformation and Fracture Mechanics of Engineering Materials, 4th ed., Wiley, Hoboken, NJ.

[25] Anderson, L. T., 2005, Fracture Mechanics, Fundamentals and Applications, 3rd ed., CRC Press, Boca Raton, FL.

[26] Somerday, B. P., 2008, "Technical Reference on Hydrogen Compatibility of Materials-Plain Carbon Ferritic Steels: C-Mn Alloys (Code 1100)," Sandia National Laboratories, Livermore, CA, Report No. SAND2008-1163.

[27] Nelson, G. H., 1976, "On the Mechanism of Hydrogen-Enhanced Crack Growth in Ferritic Steels," Second Conference on the Mechanical Behavior of Materials, Boston, MA, Aug. 16–20, pp. 690–694.

[28] Nelson, H. G., and Stein, J. E., 1973, "Gas-Phase Hydrogen Permeation Through Alpha Iron, 4130 Steel, and 304 Stainless Steel From Less Than 100 C to Near 600 C," NASA Ames Research Center, Moffett Field, CA, Technical Report No. NASA-TN-D-7265.

[29] Mao, S. X., and Li, M., 1998, "Mechanics and Thermodynamics on the Stress and Hydrogen Interaction in Crack Tip Stress Corrosion: Experiment and Theory," J. Mech. Phys. Solids, 46(6), pp. 1125–1137.

[30] Hirth, J., 1980, "Effects of Hydrogen on the Properties of Iron and Steel," Metall. Mater., Trans. A, 11(6), pp. 861–890.

[31] Amaro, R. L., Drexler, E. S., and Slifka, A. J., 2014, "Fatigue Crack Growth Modeling of Pipeline Steels in High Pressure Gaseous Hydrogen," Int. J. Fatigue, 62, pp. 249–257.

[32] Amaro, R. L., Drexler, E. S., Rustagi, N., Nanninga, N. E., Levy, Y. S., and Slifka, A. J., 2012, "Fatigue Crack Growth of Pipeline Steels in Gaseous Hydrogen-Predictive Model Calibrated to API-5 L X52," International Hydrogen Conference, Moran, WY, Sept. 9–12, pp. 329–337.

[33] Amaro, R. L., Drexler, E. S., and Slifka, A. J., 2014, "Development of an Engineering-Based Hydrogen-Assisted Fatigue Crack Growth Design Methodology for Code Implementation," ASME Paper No. PVP2014-28943.